Picosecond absorption spectroscopy of self-trapped excitons and Ce excited states in CeBr_{3} and La_{1−x}Ce_{x}Br_{3}

Peiyun Li, Sergii Gridin, K. Burak Ucer, Richard T. Williams, and Peter R. Menge

Picosecond Absorption Spectroscopy of Self-Trapped Excitons and Ce Excited States in $CeBr_3$ and $La_{1-x}Ce_xBr_3$

Peiyun Li, Sergii Gridin, K. Burak Ucer, and Richard T. Williams[*]

Department of Physics, Wake Forest University, Winston Salem, NC 27106, USA

Peter R. Menge

Saint-Gobain Crystals, 17900 Great Lakes Parkway, Hiram, OH 44234, USA

(Dated: February 20, 2019)

Transient absorption following generation of free carriers in the bulk of $CeBr_3$ shows that the Ce^{3+*} excited state responsible for scintillation light emission in this material is populated with a 10% to 90% rise time of 540 femtoseconds. The Stokes shift of luminescence from this Ce^{3+*}(4f, 5d) Frenkel exciton establishes that it is self-localized by lattice relaxation. Charge transfer transitions from the valence band to the 4f hole component of the Ce^{3+*}(4f,5d) lattice-relaxed exciton and from its 5d electron component to the conduction band are identified for the first time in $CeBr_3$. In $LaBr_3$:Ce, energy transfer from bromine-based relaxed excitons to the Ce^{3+} dopant closest to the point of exciton localization occurred in tens of picoseconds depending on Ce concentration, whereas in $CeBr_3$ the bromine-based relaxed exciton transfers energy to the Ce^{3+*}(4f,5d) exciton in 540 fs. We failed to find evidence of any significant signature of Ce^{4+}, i.e. holes trapped on Ce^{3+} ions, in excited $CeBr_3$ or $LaBr_3$:Ce in the spectral range 0.41 to 2.16 eV. The accurate time-sequencing of population in different excited-state and trapped-charge species involved in energy storage, transport, and emission after ionizing excitation is useful for understanding the fundamental mechanisms at work in scintillation as they may influence light yield, its proportionality to energy deposition, and energy resolution. Isolating the specific rise time of population in the emitting state from the other known contributors to coincidence-timing of gamma rays contributes information to the search for novel advances in ultrafast time-of-flight detection.

I.   INTRODUCTION

Two directions of active research on scintillators for advanced gamma spectroscopy and imaging aim to improve the timing resolution and the energy resolution. Recent research has pushed gamma-ray timing resolution to the 100 picosecond range, better enabling time-of-flight positron-electron tomography (TOF-PET) and offering routes for distinguishing gamma rays emanating from multiple particle collisions per bunch crossing in high energy experiments planned for the high-luminosity upgrade of the Large Hadron Collider, for example[1]. To take full advantage of time-of-flight localization along the gamma-ray path, there is strong motivation to push the timing resolution toward 10 ps[2], which will require novel approaches and detailed knowledge of separate contributions to the timing resolution limit. This study of picosecond-resolved optical absorption from excited states involved in scintillation was undertaken partly in support of the broad search for ways to improve timing resolution. It also serves the parallel search for better energy resolution of gamma ray detection by providing information on rate parameters and populations in the excited states useful for modeling fundamental mechanisms underlying energy resolution and light yield[3,4].

Time-resolved spectroscopy of absorption induced following free-carrier production in a crystal can detect population in the activator excited state that has been transferred from free carriers in the host crystal in reasonable approximation of parts of the scintillation process. In addition to the rise of population in the excited state of the activator, the same experiment can record the sequence of populations in intermediate excited-state species and/or trapped charge states leading up to the final emitting population. Part of the challenge faced in such work on a crystal is to first identify the absorption signatures of all relevant states in the sequence. Transient absorption in scintillator materials measured by subpicosecond laser pulses in a pump-probe format has been applied to CsI:Tl, NaI:Tl, SrI_2:Eu[5] and $LaBr_3$:Ce[6] in our lab. Transient absorption combined with photoluminescence rise induced by subpicosecond laser pulses and measured with a streak camera were recently applied to Ce-doped gallium gadolinium aluminum garnet (GAGG:Ce) by Tamulaitis et al[7].

$CeBr_3$ studied in this work presents one of the best prospects among spectroscopic scintillators to achieve timing resolution in the low tens of picoseconds. Coincidence timing resolution in $CeBr_3$ has been reported at 119 ps[8] and 59 ps[9] in crystals of size 1-inch diameter × 1-inch height and 4×4×5 mm³, respectively. Operation of $LaBr_3$:Ce as a scintillator necessarily involves energy transfer over some distance from the host to a Ce dopant for a significant part of its light yield. There is a two-component rise of scintillation light reported in $LaBr_3$:Ce[10–12] but not in $CeBr_3$[12].

$CeBr_3$ along with the other cerium tri-halides exhibits an unusual dichotomy of two effective band gaps and two associated excitons of quite different nature, as illustrated in Fig. 1. Vasilev, et al have previously discussed the co-existence of the fluoride-based charge-transfer excitons and cerium-based Frenkel excitons in CeF_3[13]. In

CeF$_3$, the two excitons have widely different energies such that virtually no resonant energy transfer can take place. Since there are 18 halogen valence electrons per formula unit compared to only one Ce f electron at the valence edge, more holes are produced initially in the halogen valence band than in the lone Ce 4f band. The light yield and related energy resolution of CeF$_3$ suffer the consequences[13]. In CeBr$_3$, the bromine- and cerium-based excitons have similar and spectrally overlapping energies when lattice relaxation of self-trapped excitons is taken into account, such that resonant dipole-dipole energy transfer can be expected, leading potentially to energy concentration in the Ce^{3+*} excited state as needed for scintillation. But unlike cerium-doped LaBr$_3$, where isolated Ce ions are the light emitters, in CeBr$_3$ the Ce^{3+} ions located periodically in every unit cell mean that the cerium excited state is a Frenkel exciton.

In the schematic band diagram of CeBr$_3$ in Fig. 1, we represent one valence band, VB#1, composed of fully-occupied bromine 4p orbitals, and another band about 1.2 eV higher in energy which acts effectively as VB#2, composed from the occupied lowest cerium 4f orbital. In the related crystal LaBr$_3$, which will often be compared, there are no 4f electrons in the ground state but most of the other features of band structure remain similar. A detailed band structure of LaBr$_3$ along with confirming comparisons to experiment, has been given by Aberg et al[14] Approximately 5.9 eV[15] above the bromine-based valence band edge in LaBr$_3$ (at low T) is the conduction band dominated by La5d orbitals with minor Br4d and La4f contributions[14]. Similarly, the low-temperature band gap of CeBr$_3$ is about 5.8 eV[16] and the conduction band can be expected to contain dominant Ce5d and minor Br4d and Ce4f contributions analogous to the LaBr$_3$ conduction band.

The basis for what should "reasonably be expected" for excitation-induced states in the gap lies partly in analogy to results of very extensive studies of self-trapped excitons (STE) in the reasonably similar metal halide materials, alkali halides. An important bridge to STE structure in the rare-earth tri-halides of present concern is provided by recent first-principles calculations of Canning et al[17]. They found Br$_2^-$ V$_k$ centers and V$_k$-based STEs in LaBr$_3$ with three stages of off-center relaxation of the STEs, conceptually analogous to well known off-center relaxed STEs in alkali halides. Therefore we have borrowed the main model and nomenclature of STE lattice relaxation from alkali halides (also alkaline-earth halides) to discuss and illustrate our observations on CeBr$_3$, LaBr$_3$, and LaBr$_3$:Ce.

We present lattice-relaxed (self-trapped) bromine-based excitons in the left half, and cerium-based Frenkel excitons in CeBr$_3$ in the right half of Fig.1. We have chosen to represent excitons by showing levels of the electron and hole states involved, with a dashed ellipse drawn to remind us that there is coulomb attraction and associated correlation in the exciton. It is not an exact or necessarily favored representation, but is appropriate because
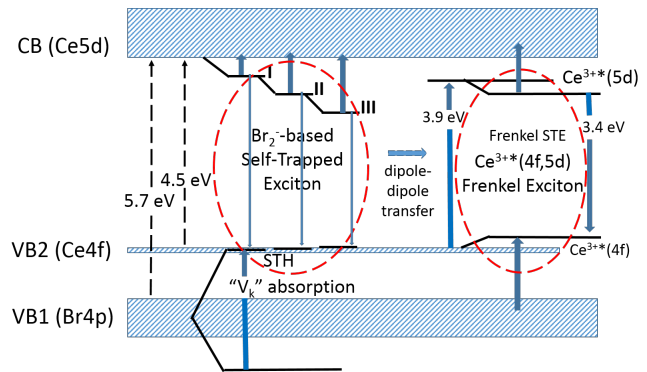

FIG. 1. Schematic representation of energy bands around the fundamental gap in CeBr$_3$ and two types of excitons supported: Bromine-based charge transfer excitons on the left and cerium-based Frenkel excitons on the right. Excitons are indicated by showing the contributing electron and hole states connected by a dashed ellipse meant to remind us of the Coulomb binding and consequent correlation between the electron and hole. This inexact representation was chosen because it allows representation of optical transitions of the electron and hole components of the self-trapped excitons to neighboring bands which are the basis of many observed transitions in our picosecond absorption spectroscopy.

the charge transfer (CT) absorption bands that comprise much of our excitation-induced spectra are in first order separate excitations of the electron component or the hole component of the respective excitons. Upward blue arrows in Fig. 1 represent CT absorption transitions (a) promoting the bound electron in bromine-based STEs on the left and cerium-based Frenkel STEs on the right into the conduction band, (b) promoting a valence electron into the 4f hole component of the cerium-based Frenkel STE at the lower right, and (c) the well-known V$_k$-type absorption band transition filling the self-trapped hole (STH) on a bonded Br$_2^-$ pair from a deeper localized bonding state. Radiative decay of the Ce^{3+*}(4f,5d) self-trapped Frenkel exciton is the useful transition for scintillation of CeBr$_3$. Near-field coupling of the radiative and absorbing dipole transitions is the basis for dipole-dipole energy transfer suggested as a possibility in Fig. 1.

The notation I, II, and III in the upper left part of the bandgap in Fig. 1 is shorthand notation of no off-center relaxation, moderate off-center relaxation and strong off-center relaxation of STEs established first in alkali halides but found in analogous versions by experiment and calculation in other metal halides including LaBr$_3$[17]. Off-center refers to displacement of the electron wavefunction centroid relative to the hole wavefunction centroid. It has been well established that the larger the off-center relaxation, the more the bound-electron wavefunction in the STE comes to resemble that of an F center, occupying the energetically favorable halide vacancy that opens up as the halogen atom (bearing the hole) moves toward an interstitial site. Consequently the more

off-center, the deeper the electron binding below the conduction band. This has been reviewed elsewhere[18] and we will not review the alkali halide example further.

II. EXPERIMENTAL METHOD

The laser system comprises a Ti-sapphire oscillator and regenerative amplifier producing pulses at 840 nm with 300 fs pulse duration and about 3 mJ pulse energy at 10 Hz. Specifically the system uses a Coherent Verdi G7 diode driven continuous laser pumping a Coherent Mira 900 mode-locked oscillator whose output is amplified in a Positive Light regenerative cavity followed by a double-pass final power amplifier before recompression. The pulse is split to generate 2nd harmonic (420 nm, 2.95 eV) and 3rd harmonic (280 nm, 4.43 eV) pump pulses which can produce two-photon absorption across the band gaps of $CeBr_3$ and $LaBr_3$ creating electron-hole pairs, or other excitations as described following. Two-photon absorption used for excitation in this experiment allows interband excitation of free electrons and holes to be produced in the bulk of the sample, in some ways approximating results of gamma-ray stopping better than by direct absorption of interband light at the surface of the crystal. The energy per pulse of the pump beam is measured to be $60 \mu J$ at the sample, giving an irradiance of approximately 10^{12} W/cm^2. This irradiance is chosen to produce $\sim 10^{18}$ electron-hole pairs per cm^3 at the soft focus, similar to densities produced in the ~ 100 keV portion of a photoelectron track. The two-photon final state excitation at 5.9 eV produced by the 2nd harmonic pulse exceeds the $CeBr_3$ room temperature band gap of 5.7 eV, so free carriers are produced although not the very hot carriers produced by gamma-ray stopping.

When a $LaBr_3$ sample is doped with 4% or 20% Ce for example, the 4.43-eV 3rd harmonic photons are strongly absorbed by Ce^{3+} (4f-5d transitions) before the beam can come to a sufficient focus to produce 2-photon interband excitation. We used this as a method to see effects of direct excitation of isolated Ce^{3+} ions in $LaBr_3$:Ce[6]. Figure 2 displays the luminescence excitation spectrum of $CeBr_3$[19] along with the absorption spectrum of the $CeBr_3$ sample studied in this work and absorption of a thin film of $CeBr_3$[16]. Vertical dashed lines at 2.95 and 4.43 eV indicate the photon energies of the 2nd and 3rd harmonics of our Ti-sapphire laser with respect to absorption in $CeBr_3$. Because of damage by the 4.43-eV light in pure $CeBr_3$, only the 2.95-eV photons producing two-photon absorption above the gap were used for $CeBr_3$.

The $CeBr_3$ crystal was grown by Saint-Gobain Crystals. The sample was cut, polished, and sealed in a hermetic enclosure with fused quartz windows under dry glove box conditions while at Saint-Gobain. The tunable probe pulse for pump-probe measurements was generated by an optical parametric amplifier (OPA) and its frequency-doubled output. A PbS detector was used
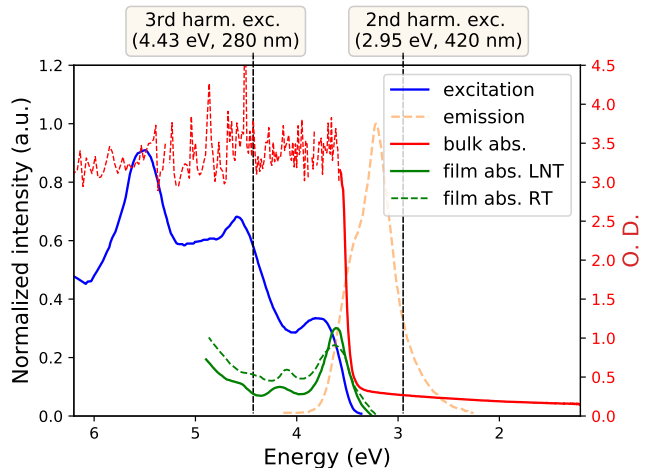

FIG. 2. The solid blue curve and orange dashed curve are excitation and emission spectra, respectively, measured on single-crystal $CeBr_3$ at 300 K[19]. The solid red curve is absorption of the 3-mm thickness sample of single-crystal $CeBr_3$ used in this study (Optical Density scale on the right). The solid green and dashed green curves are absorption of evaporated thin-film $CeBr_3$ at 78 K and room temperature, respectively, replotted from[16]. The thin film absorption coefficient measured by Sato is approximately 10^4 cm^{-1} at the peak of the 3.6-eV band, not represented to scale in Fig. 1.

from 1000 nm to 3025 nm and a biased Si photodiode for wavelengths below 1000 nm. In this way, wavelengths from 575 nm to 3025 nm (2.16 eV to 0.41 eV) could be measured. Time-delay data with this method were of good quality over the 0-170 ps range for each wavelength. Changing wavelength to acquire spectra requires that the OPA be re-tuned for each wavelength, followed by pump/probe spot realignment as well. This was a source of possible noise from wavelength to wavelength in the spectra, and indeed there is a streakiness in the spectra.

III. RESULTS AND DISCUSSION

A. Comparisons of induced optical response across the $La_{1-x}Ce_xBr_3$ composition series

Figure 3 shows time-resolved spectra of induced absorption from 0.41 to 2.16 eV and 0 to 170 ps following excitation of $La_{1-x}Ce_xBr_3$ for x=0.004%, 4.4%, 22.2%, and 100%. Fig. 3 was measured after two-photon interband excitation of the host $LaBr_3$ and the bulk crystal $CeBr_3$ by 420 nm (2.95 eV) photons which do not directly (one-photon) excite the Ce(4f-5d) transitions. In the left three panels for $LaBr_3$ and $LaBr_3$:Ce excited in the host matrix, we identified the absorption bands centered at 0.46 eV and about 0.9 eV as due to self-trapped excitons with Type I (on-center) and Type II (moderately off-center) relaxation, respectively[6]. It was sug-
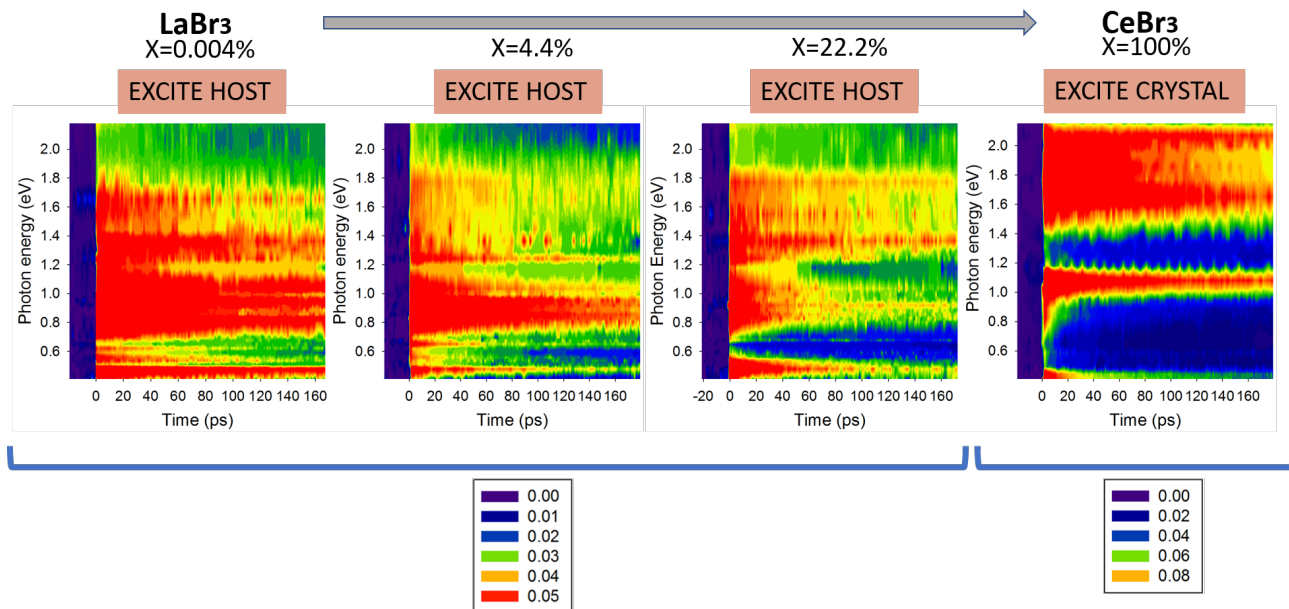
FIG. 3. Absorption induced by the pump pulse is displayed versus probe delay from 0 to 170 ps and versus probe photon energy from 0.41 to 2.16 eV. The samples are $La_{1-x}Ce_xBr_3$, where x is indicated at top. Labels above eavch color map indicate that the pump pulse (2.95-eV) excites the host or pure crystal by two-photon interband absorption, not Ce directly in a one-photon process.

gested that some of the absorption centered around 1.4 eV may be due to Type III (strongly off-center) STEs. The optical transitions are illustrated in the schematic band diagram of Fig. 1 as photoionization of the bound-electron component of the STE upward into or approaching the conduction band. First-principles theoretical calculations on STEs in $LaBr_3$ have found three stable or metastable minima (I, II, III) at each of two of the three inequivalent bromine sites in the $LaBr_3$ unit cell[17]. Inequivalent anion sites is an added complexity in $LaBr_3$ and $CeBr_3$compared to alkali halides, and may account for some of the multi-band complexity comprising each of the three main envelopes of induced absorption bands in Fig. 3. The decay of the three envelope bands of absorption becomes faster with greater Ce concentration, and this dependence was attributed to dipole-dipole transfer from host STE to Ce dopant before STE thermal migration can occur[6]. The V_k-type ultraviolet absorption of the self-trapped hole component of the STE was also observed in host-excited $LaBr_3$, corresponding to the schematic representation in the lower left of Fig. 1.

The right-hand panel for pure $CeBr_3$ in Fig. 3 is quite different in character from the three $LaBr_3$ spectra on the left. The three band envelopes in the left panels centered at 0.47, 0.9, and 1.4 eV are replaced in $CeBr_3$ by two envelopes or bands at about 1.8 eV and 1.05 eV which decay more slowly and are considerably stronger. Note the change of color map range for $CeBr_3$. There is a very fast-decaying shoulder in $CeBr_3$ at about 0.9 eV and a fast-decaying band at about 0.44 eV which correspond in energy to bromine-based STE bands in the host-excited

$LaBr_3$ but decay much faster in $CeBr_3$.

To suggest origins of the new induced absorption bands in excited $CeBr_3$, we look at Fig. 4 which compares the $CeBr_3$ spectrum on the right to two $LaBr_3$:Ce samples in the middle that were excited by one-photon absorption directly in the $Ce^{3+}(4f-5d)$ transition producing the dopant excited state $Ce^{3+*}(4f,5d)$. Comparing the first and second panels for 4.4% Ce-doped $LaBr_3$ excited in the host and on the dopant respectively, shows clearly that the three low-energy band envelopes of host STE transitions is swapped out to be replaced by longer lived higher-energy bands at about 2.1 eV and 1.3 eV when Ce is directly excited. In these color-map spectra, the host-excited $LaBr_3$:Ce(4.4%) is blue at the top and red at the bottom, while the direct Ce-excited $LaBr_3$:Ce(4.4%) is red at the top and blue at the bottom. Continuing across the 2nd, 3rd, and 4th panels of Fig. 4 shows that as Ce concentration increases, the band at the top becomes progressively stronger. The induced absorption near 2.1 eV is due to excited cerium. We have argued that the 2.1-eV transition energy in $LaBr_3$:Ce is 5d electron photoionization from $Ce^{3+*}(4f,5d)$[6].

To compare Ce CT transition energies to band edges in $LaBr_3$:Ce and $CeBr_3$, it is useful to look again at Fig. 1 which suggests where the $Ce^{3+}4f$ electron occupied level is located relative to the bromine-based valence band edge in $CeBr_3$ versus $LaBr_3$:Ce. Dorenbos has developed a chemical shift model of vacuum-referenced 4f electron binding energies across many hosts and used it to estimate that the ground-state 4f level of Ce dopant in $LaBr_3$ is about 0.5 eV above the valence band edge[20].
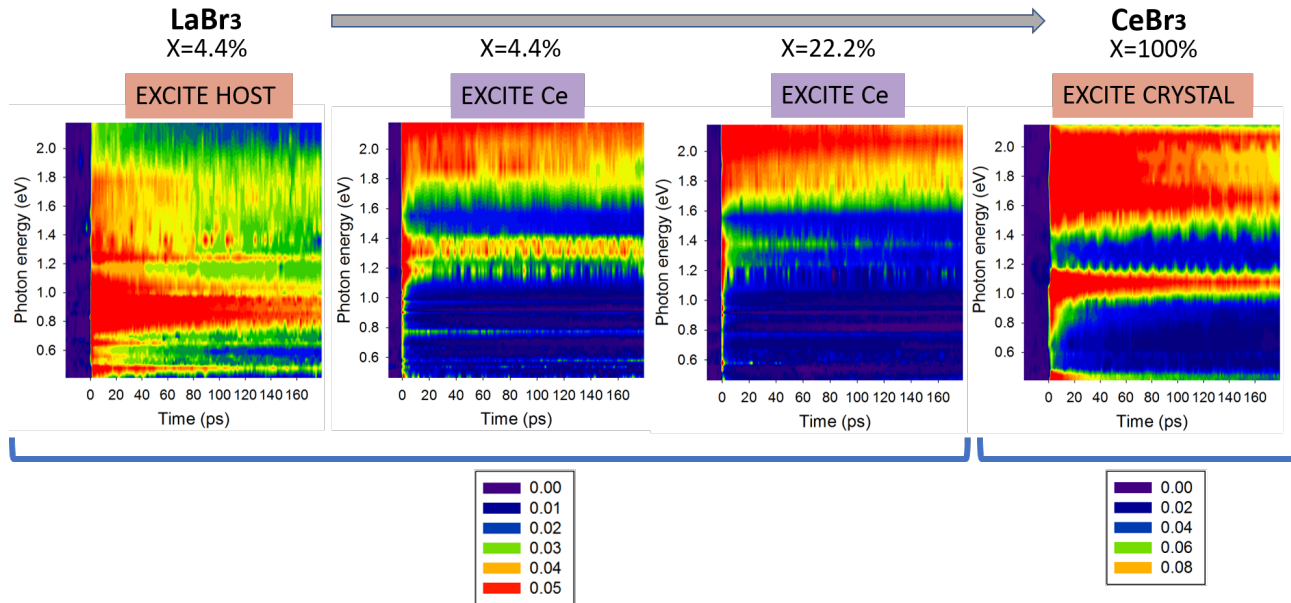
FIG. 4. Absorption induced by the pump pulse is displayed versus probe delay from 0 to 170 ps and versus probe photon energy from 0.41 to 2.16 eV. The samples are $La_{1-x}Ce_xBr_3$, where x is indicated at top. Labels above each color map indicate that the pump pulse (2.95-eV 2nd harmonic in panels 1&4, 4.43-eV 3rd harmonic in panels 2&3) excites the host, pure crystal, or Ce directly.

That 4f placement was used in our analysis of induced picosecond absorption bands of isolated Ce in $LaBr_3$:Ce such as the middle two panels in Fig. 4. In Fig. 1 we have taken the occupied Ce 4f band in $CeBr_3$ to be 1.2 eV above the bromine-based valence band edge, 0.7 eV higher than the Dorenbos estimate for $LaBr_3$:Ce. Some of the experimental data that we cite to support the 1.2 eV estimated Ce4f-placement in $CeBr_3$ are represented in Fig. 2.

Sato measured the optical absorption of thin-film samples of $LaBr_3$ and $CeBr_3$. His analysis shows that the spectral features that can be attributed to interband transitions from the bromine-based valence bands to the conduction bands and associated excitons occur at the same energy in $LaBr_3$ and $CeBr_3$ to within about 0.1 eV[16]. The gap from bromine-based valence band to conduction band is about 5.7 eV in $CeBr_3$ vs 5.8 eV in $LaBr_3$ at room temperature. The same measurements showed that only in the case of $CeBr_3$, there were absorption bands at 3.6 eV, ~4.15 eV, and a rise starting from ~4.4 eV. The spectra are reproduced from Sato's data in Fig. 2 as the green solid and dotted curves for 78 K and 295 K respectively. Sato attributed this absorption to Ce in $CeBr_3$. The peak absorption coefficient of the 3.6 eV band was $\alpha \approx 10^4$ cm^{-1}. This is quite a high absorption coefficient relative to usual impurities or defects, and approaches the low end of values associated with exciton peaks. We suggest that the 3.6 eV absorption peak could be formation of a Ce^{3+*}(4f,5d) Frenkel exciton, and the rise from 4.4 eV may be the onset of transitions from Ce4f to the conduction band. Figure. 2 also reproduces

the excitation spectrum of Ce^{3+*} luminescence in crystal $CeBr_3$ at room temperature measured by Drosdowski et al[19]. We are struck by the near correspondence of the 3.8 eV peak in the Drosdowski excitation spectrum of a crystal and the 3.6 eV thin film spectrum of Sato. The small relative peak shift could be due to use of an evaporated film by Sato and single crystal by Drosdowski et al. We propose that the large peaks in the excitation spectrum of 2 centered at 4.6 eV and 5.7 eV derive from transitions of electrons into the conduction band from initial states in the Ce4f and Br4p valence bands respectively. Exciton peaks and strong band-to-band density-of-states features typically appear in luminescence excitation spectra on the low energy side of the actual absorption peaks due to surface quenching. In constructing Fig. 1, we therefore took Frenkel exciton creation to be represented at 3.9 eV on the 3.8 eV Drosdowski peak. This is 0.1 eV lower than the 4.0 eV Ce(4f-5d) absorption peak of isolated Ce in $LaBr_3$:Ce[15]. Our 3.9 eV assignment is a symbolic allowance for the fact that the Ce Frenkel exciton should be lower energy than the isolated Ce ion excited state because of exciton band dispersion. The start of transitions from Ce4f to the conduction band at about 4.5 eV in the Fig.2 excitation spectrum is labeled on the left side of Fig. 1. Subtracting this cerium-based band gap from the bromine-based band gap of 5.7 eV puts Ce4f at 1.2 eV above the bromine-based valence band in the estimate of $CeBr_3$ drawn in Fig. 1. The unrelaxed Frenkel exciton then is 0.6 eV below the conduction band. We should note that this interpretation of the excitation spectrum[19] is not the same as was suggested by Drosdowski et al.

Their suggested peak assignments ascribed the 4.6 eV peak to the lowest 4f-5d excitation of Ce. This is considerably higher than 4 eV measured for the 4f-5d excitation of Ce dopant in LaBr$_3$:Ce, which seems problematic in our opinion. Modification of the 3.8-eV peak in the excitation spectrum by heat treatment does not disqualify it from being a Ce Frenkel exciton[19]. Sato also measured X-ray Photoelectron Spectra (XPS) of films of LaBr$_3$ and CeBr$_3$. Comparison reveals a feature ascribable to occupied Ce4f in CeBr$_3$ that is roughly in the range of 1 eV above what might be considered the bromine 4p edge, though resolution was not high. It may also be noted that band structure calculations for CeBr$_3$ using DFT + U found the occupied 4f band to be 56% of the way up from the top of the Br4p valence band to the bottom of the Ce5d conduction band[21]. Given an experimental band gap of 5.7 eV, this would translate to the occupied Ce4f band being 3.2 eV above the Br valence band and 2.5 eV below the conduction band. That is closer to the conduction band than can be consistent with the transmission spectrum of CeBr$_3$ in Fig. 2, but the point is that DFT + U was indicating the occupied Ce 4f band fairly high in the gap of CeBr$_3$ rather than very close to the bromine valence band as for isolated dopant Ce in LaBr$_3$:Ce predicted by the chemical shift model[22]. There is a difference between Ce as an isolated dopant and Ce as a periodic component of a crystal. There can be no concept of Ce*(5d) excited states in CeBr$_3$ that are not part of an exciton or in the conduction band.

Proceeding on the basis of the CeBr$_3$ bands as diagramed in Fig. 2, we take into account the measured ~ 0.45-eV Stokes-shift of Ce^{3+*} luminescence[19], and consider it as shared 0.25-eV self-trapping relaxation energies in the electron and hole components of the exciton. The CT transitions to the bands will be from these relaxed electron and hole levels. In Fig. 1, the 1-eV electron photoionization band peak assignment is reasonable considering that the density of states (DOS) rises from each band edge. The 1.7 eV envelope center of valence-electron excitation into the relaxed 4f hole in the Frenkel STE is consistent with Fig. 1 as diagrammed. Widths and shapes of the CT band envelopes might derive from DOS features of the bands. The decay times of CT absorption transitions to both free-carrier bands from the same Ce^{3+*}(4f,5d) exciton should be the same rate, which is consistent with the measured 1.05 and 1.7-eV band envelopes. In our opinion, this fact argues against one of them being instead the CT absorption band of a Ce^{4+} trapped hole, which is unlikely to share a common decay with Ce^{3+*}. We conclude that a significant signature of Ce^{4+} CT absorption which would imply production of a significant population of Ce^{4+} trapped holes following electron-hole pair production by two-photon excitation in this experiment has not been found in the 0.41 to 2.16-eV spectral range in CeBr$_3$. Earlier studies by the same method on LaBr$_3$ and LaBr$_3$:Ce reached the same conclusion. Two possible reasons for this finding are the 18 -to 1 ratio of Br4p valence electrons to Ce4f va-

lence electrons, and the relative capture cross sections of the positive Coulombic Self-Trapped Hole (STH) versus the site-neutral trapped Ce^{3+} in a sublattice of tri-valent rare earths. The key points are that the initial excitation is less likely to produce holes on Ce than on Br, and that after electrons and holes are produced, capture of electrons on holes to produce STE is Coulombically promoted whereas hole capture on Ce^{3+} lacks long-range Coulomb attraction. The fact that excitons are produced in preference to trapped charge carriers, suggests that scintillation in both crystals is dominated by STE formation and energy transfer rather than binary recombination of charge carriers on cerium. That in turn determines the kinetic order of recombination and a great deal about proportionality of light yield and of energy resolution at the fundamental level of modeling and possible material engineering.

Figure 5 shows the CeBr$_3$ data measured on the faster time scale of 0-15 ps. It presents independent measurements taken at a higher density of pump-probe time delays, not simply a re-scaling of the time axis for the data of Fig. 4.
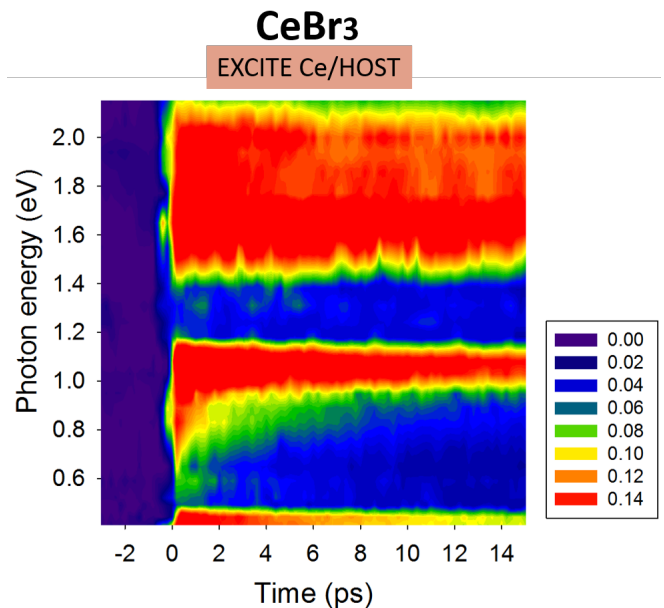

FIG. 5. Absorption induced by the pump pulse is displayed versus probe delay from 0 to 15 ps and versus probe photon energy from 0.41 to 2.16 eV in CeBr$_3$ after electron-hole pair generation by two-photon absorption (2 × 2.95 eV).

This faster view of the 1.8 and 1.05 eV CT bands involving the Ce^{3+*}(4f,5d) exciton in CeBr$_3$ makes it clear that the population in the responsible Ce^{3+*}(4f,5d) exciton state achieves its maximum occupancy in less than 1 picosecond. To appreciate some details of what is involved in that, we focus attention on the low-energy shoulder of the 1.05-eV band. The shoulder may be considered to have its center around 0.9 eV. We propose that it is the pure-CeBr$_3$ version of the 0.9 eV Type II

bromine-based STE seen already in LaBr$_3$ and LaBr$_3$:Ce. In Fig. 3, the relatively long-lived STE absorption at 0.9 eV in LaBr$_3$ projects straight across the panels with increasing Ce concentration and increasing decay rate of 0.9-eV absorption to a 0.9 eV short-lived shoulder on the long-lived band at 1.05 eV in CeBr$_3$. The identified shoulder at 0.9 eV has an approximate 1-ps lifetime. This is similar to the lifetime of the corresponding spectral band observed for direct Ce multiphoton excitation in Ce-doped LaBr$_3$[6], where it was concluded that 1 ps is the transfer time time from a bromine-based STE to a nearest-neighbor Ce^{3+}.

The data of Fig. 5 have been averaged over photon energies lying within the two major spectral bands, and the mean induced absorption plotted as conventional rise and decay curves in Fig. 6. Figure 6 shows the 10% to 90% rise time of the Ce^{3+*} population measured by its CT absorption at 1.02 eV to be 540 femtoseconds. Deconvoluting the 300 fs pulse width implies an approximate 300 femtosecond Ce^{3+*} population time from 10% to 90% when the excitation was deposited as valence interband excitation, not primarily direct excitation of Ce. It is not the same as in gamma ray excitation because those carriers are hotter initially, and are created in spatial gradients. But neither is it simple photoexcitation of Ce. The carriers created independently and primarily by bromine excitation must get to a cerium excited state eventually in the form of an exciton in CeBr$_3$. This has a lot in common with a subset of what occurs in scintillation, and we have described an experiment that can measure it with subpicosecond resolution.
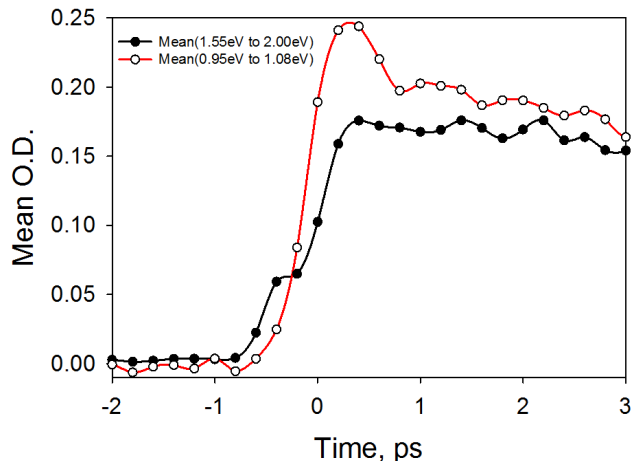

FIG. 6. The data of Fig. 6 have been averaged over photon energies lying within the two major spectral bands, and the mean induced absorption is plotted versus time. The pump-probe coincidence (t = 0) was not determined absolutely independent of the absorption measurement. The t = 0 is placed at the 50% point on the rising edge.

The rise of absorption in the 1.8 eV band appears slower, with 10% to 90% rise time of 830 fs, but that includes the feature appearing as a bump at the beginning of the rise. Looking at the spectral data from which these plots came in Fig. 5, the bump can be seen to come from the weak but very early features at 1.65 eV and 2.0 eV. We can also see that one other early bump at 0.88 eV was missed in the photon energy range 0.95-1.08 eV chosen and averaged to represent the main band near 1 eV which we associate with Ce^{3+*} CT. The 0.88 eV early bump in 5 is at the center of what we can imagine to be a short-lived band comprising the low-energy shoulder on the 1-eV band. We discussed this shoulder from the aspect of spectrum just above, noting its energy correspondence with the 0.9 eV band of bromine-based STE (Type II) in LaBr$_3$. Another candidate for a feature that could appear essentially instantaneously with the pump pulse would be two-photon excitation of the Ce4f electron directly, creating an instant Ce4f hole. We won't push the speculation further than noting that this could be a possibility for the early (and weak) bumps at 1.65 and 2 eV in Fig. 5.

B. Dipole-dipole transfer STE → Ce^{3+*} and Ce^{3+*} persistence to nanosecond range

The left 3 panels in Fig. 3 were analyzed for STE decay time in Ref.[6], finding that in undoped, 4.4%-, and 22.2%-doped LaBr$_3$:Ce, about 50% of the absorption decayed with time constants of 92 ps, 69 ps, and 38 ps, respectively versus Ce concentration. The increase of STE decay rate with Ce concentration is clear, and was interpreted as indicating energy transfer from Br$_2^-$ STEs to Ce^{3+} dopant ions within the effective dipole-dipole transfer radius of STEs at their place of creation in the host lattice. This last stipulation comes from the tens of picosecond transfer rate being faster than would be expected from hopping transport of the STEs. STE diffusion should characterize the part of energy transfer to Ce activators from the roughly 50% of STEs that decay more slowly than could be measured in this experiment. That slower transfer component was studied particularly in the luminescence and scintillation experiments of Bizzari and Dorenbos[23]. We suggest that the 92 ps decay time of 50% of STEs in the undoped LaBr$_3$ may be the dipole-dipole quenching rate of STEs with themselves under conditions of our picosecond absorption measurement, in which electron-hole pairs are created at a density of roughly 10^{18} e-h/cm^3.

To relate the transient absorption measurements most directly to scintillation, the absorption measurements of the Ce^{3+*} excited state should extend into the range of one or a few nanoseconds where scintillation detectors operate. We found nanosecond-range time-delay measurements to be more difficult than the picosecond range in our experiments, due to reasons which included some spatial incoherence in the "delayed" (advanced) pump beam as well as curvature in the rails of longer translation stages. Nevertheless, decay-time measurements in

CeBr$_3$ to 1.2 ns were measured and are shown in Fig. 7. Corresponding nanosecond observations were reported for LaBr$_3$ and LaBr$_3$:Ce in Ref.[6].

According to the previous discussion and Fig. 1, the absorption in CeBr$_3$ in Fig. 7 from about 1.5 to 2.1 eV is attributed to Ce^{3+*}(5d) VBCT transitions, the absorption at 1.06 eV to Ce^{3+*} CBCT, and the band at 0.43 eV to bromine-based STE Type I. After a rapid decay which could indicate dipole-dipole quenching of close Ce^{3+*} and STE pairs, the absorption appears stable out to 1.2 ns. Data using different portions of the optical delay translation stage indicated that the undulations come from curvature in the ways.
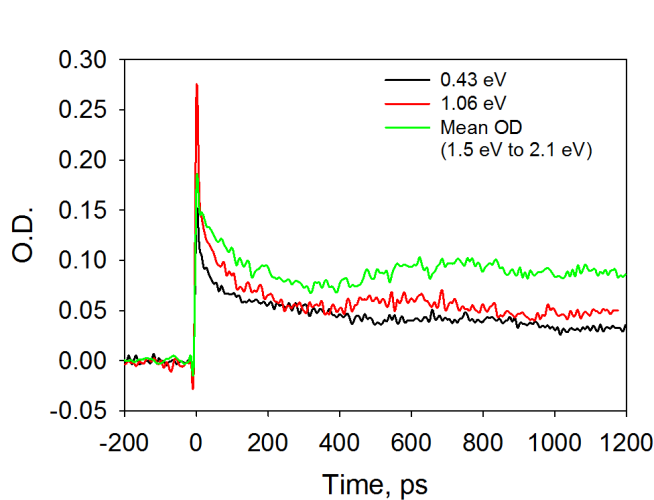

FIG. 7. Transient absorption decay plots in CeBr$_3$ at 0.44 eV, 1.06 eV, and averaged from 1.65 to 2.07 eV, measured from 0 to 1200 ps.

C. Comparing scintillation rise time with rise of population in the emitting level, Ce^{3+*}

Fast measurements of scintillation rise time of LaBr$_3$:Ce[10–12], the rise[12] and decay times[12,24] of CeBr$_3$, and pulse timing with CeBr$_3$[8,9] have been reported. Glodo et al showed that the scintillation rise time in LaBr$_3$:Ce depends on Ce concentration, with the dominant rise component varying from 15 ns at 0.5% to 380 ps at 5%, to 160 ps at 20% Ce. The rise had a fast and a slower component distinguishable at lower Ce concentrations. Seifert et al measured the rise of scintillation in LaBr$_3$:Ce(5%), finding similar two components (and stated fractional strengths) of 270 ps fast rise (strength 72%), 2 ns slower rise (strength 26%), and a very weak, slow rise of 130 ns (strength 2%), the latter of which they suggested came from carrier de-trapping[11]. D. ter Weele et al measured fast and slower rise times of 184 ps and 1.05 ns in LaBr$_3$:Ce(5%) excited with x-rays of energy $\leqslant$ 40 keV which have a small depth of interaction[12]. The fast subnanosecond rise of scintillation in LaBr$_3$:Ce should originate from the "prompt"[23] rise of population in Ce^{3+*}, which we measured indirectly to be 69 ps and 38 ps in 4.4% and 22% Ce-doped samples, respectively[6]. The 2-ns rise of scintillation in 5% Ce-doped LaBr$_3$ should originate from the transport of STEs to the dilute Ce activators, termed slow Process II by Bizarri and Dorenbos[23]. Thus in LaBr$_3$:Ce, both the prompt picosecond-scale rise and the slower nanosecond-scale rise components depend on Ce concentration via the range dependence of dipole-dipole transfer[6] and the range dependence of STE diffusive transport[23] respectively. Variable range to the closest Ce ion ceases to be an issue in CeBr$_3$. The picosecond absorption data as interpreted in this study point to a main rise time of Ce^{3+*} population in CeBr$_3$ of less than 0.54 ps.

With current applications for picosecond-scale fast timing of scintillation under intensive study[1,25,26], the prospect of striving toward thick-film or double-ended gamma detection timing that might be limited ultimately by 0.54 ps (CeBr$_3$) and 69 ps (LaBr$_3$:Ce(4.4%)) population rise compared to 161 ps and 184 ps currently measured scintillation rise[12] motivates continuing consideration of what goes on between population rise in the emitting state and the rise of detected scintillation photons. One class of those processes contains light pulse transport through the finite sample to the detector, and another one, not unrelated, is named separately as self-absorption and re-emission of the scintillation light, or generally velocity of light including group dispersion in all cases and exciton-polariton effects when present.

Fraile et al[8] measured 119 ps timing resolution with a 1"Φ x 1" CeBr$_3$ crystal. They noted in comparison that Wiener et al[9] had measured 59 ps timing resolution "for a tiny $4 \times 4 \times 5$ mm^3 CeBr$_3$ crystal". The logic of these comparisons points to a closing of the difference between measurements of rise time of population in the emissive Ce^{3+*} level deduced from picosecond absorption and the rise time and amplitude (related to coincidence timing resolution) of scintillation itself, as the crystal size is decreased to suppress time-spreading from different optical collection paths, and self-absorption and re-emission. The two measurements should become effectively equal approaching infinitesimal crystal size, which in a practical sense would have to be a single Ce^{3+*} excited ion.

Limits on coincidence timing resolution have been discussed by Derenzo[25] and others[11,27]. What the present experiments bring to the considerations is the first measurement of the rise-time of population in the emitting state, which is different from the rise-time of scintillation light at the detector. We have seen that the former can be less than a picosecond, whereas the latter depends on sample size and may not be much less than about 70 picoseconds for normal scintillator size. The initial rate of increase of scintillation light at the detector, which can be represented in terms of the scintillation rise time, decay time, pulse amplitude, and spread of optical path lengths is the main determiner of the coincidence timing resolution[25]. The difference between rise-time of popu-

lation in the emitting state and rise-time of scintillation light at the detector results mainly from two aspects of light transport in the scintillator. The first is the spread of transport times at a given speed of light from gamma interaction locations randomly throughout the scintillator volume, propagating to a single detector. Derenzo has pointed out that using a double-ended scintillator with two photodetectors to pin down the location of each gamma stopping event could allow correction of this aspect of transport spread down to at least 10 ps[25]. The second aspect of scintillation transport considered here is absorption and re-emission of the scintillation light in cases of small Stokes shift, which introduces a probabilistic variability of what the delay in re-emission is for a given photon and thus spreads the rising edge of detected scintillation in a way that cannot be fully corrected by double-ended detection. If these spreading factors can be avoided or minimized by novel design, then the ultimate limit of time to populate the emitting state such as measured in this experiment becomes most relevant.

IV. CONCLUSIONS

Charge transfer absorption transitions from the valence band into the 4f hole of the $Ce^{3+*}(4f,5d)$ excited state and likewise of its bound 5d electron into the conduction band are observed and identified in $CeBr_3$ for the first time. Time dependence of these signals gives a doubly-identified history of population in the Ce^{3+*} excited state responsible for scintillation, showing that it reaches its maximum within less than 1 ps of free-carrier generation in the bulk crystal by two-photon excitation. Its 10% to 90% rise time is 540 femtoseconds. The Ce^{3+*} luminescent state in $CeBr_3$ is shown to be a self-trapped Frenkel exciton, which receives population from initially created bromine-based STEs, by a process attributed to dipole-dipole transfer. Similar dipole-dipole transfer from bromine-based STEs to Ce^{3+*} dopant states has been demonstrated in $LaBr_3$:Ce, but at more than $10\times$ slower rate because the transfer in $LaBr_3$:Ce is averaged over several spacings within the dipole-dipole range R_{dd}

≈ 3 nm (typical) whereas in $CeBr_3$ every transfer is at the nearest-neighbor ion spacing of about 0.3 nm. We found no significant signature of a Ce^{4+} CT absorption that would imply production of a significant population of Ce^{4+} trapped holes following electron-hole pair production by two-photon excitation in this experiment, within the 0.41 to 2.16-eV spectral range in $CeBr_3$. Earlier studies by the same method on $LaBr_3$ and $LaBr_3$:Ce reached the same conclusion for that system[6]. Instead, sub-picosecond formation of bromine-based STEs and also Ce-based STEs in $CeBr_3$ is observed, suggesting that scintillation in both crystals is dominated by STE formation and energy transfer rather than binary recombination of charge carriers on cerium. That in turn determines a great deal about proportionality of light yield and of energy resolution at the fundamental level of modeling and possible material engineering.

These picosecond time-resolved absorption measurements provide an interlinked set of first-time data on the unusual case of $CeBr_3$ with its two co-existing types of excitons. $CeBr_3$ is a useful scintillator with some outstanding properties and potential for fast timing. Detailed knowledge of population in key excited states and their transformations over time should be helpful for material engineering to improve light yield and energy resolution as well as exploring possible ways to exploit the very fast rise time of the Ce^* emitting state population.

[*] williams@wfu.edu

[1] P. Lecoq, IEEE Transactions on Nuclear Science **59**, 2313 (2012).

[2] P. Lecoq, IEEE Transactions on Radiation and Plasma Medical Sciences **1**, 473 (2017).

[3] X. Lu, Q. Li, G. A. Bizarri, K. Yang, M. R. Mayhugh, P. R. Menge, and R. T. Williams, Phys. Rev. B **92**, 115207 (2015).

[4] X. Lu, S. Gridin, R. T. Williams, M. R. Mayhugh, A. Gektin, A. Syntfeld-Kazuch, L. Swiderski, and M. Moszynski, Phys. Rev. Applied **7**, 014007 (2017).

[5] K. B. Ucer, G. Bizarri, A. Burger, A. Gektin, L. Trefilova, and R. T. Williams, Phys. Rev. B **89**, 165112 (2014).

[6] P. Li, S. Gridin, K. B. Ucer, R. T. Williams, and P. R. Menge, Phys. Rev. B **97**, 144303 (2018).

[7] G. Tamulaitis, A. Vaitkevičius, S. Nargelas, R. Augulis, V. Gulbinas, P. Bohacek, M. Nikl, A. Borisevich, A. Fedorov, M. Korjik, and E. Auffray, Nuclear Instruments and Methods in Physics Research Section A: Accelerators, Spectrometers, Detectors and Associated Equipment **870**, 25 (2017).

[8] L. Fraile, H. Mach, V. Vedia, B. Olaizola, V. Paziy, E. Picado, and J. Udías, Nuclear Inst. and Methods in Physics Research, A **701**, 235 (2013).

[9] R. I. Wiener, M. Kaul, S. Surti, and J. S. Karp, in *IEEE Nuclear Science Symposuim Medical Imaging Conference*

(2010) pp. 1991–1995.

[10] J. Glodo, W. W. Moses, W. M. Higgins, E. V. D. van Loef, P. Wong, S. E. Derenzo, M. J. Weber, and K. S. Shah, IEEE Transactions on Nuclear Science **52**, 1805 (2005).

[11] S. Seifert, J. H. L. Steenbergen, H. T. van Dam, and D. R. Schaart, Journal of Instrumentation **7**, P09004 (2012).

[12] D. N. ter Weele, D. R. Schaart, and P. Dorenbos, Nuclear Instruments and Methods in Physics Research Section A: Accelerators, Spectrometers, Detectors and Associated Equipment **767**, 206 (2014).

[13] A. N. Belsky, I. A. Kamenskikh, V. V. Mikhailin, C. Pedrini, and A. N. Vasil'ev, Radiation Effects and Defects in Solids **150**, 1 (1999), https://doi.org/10.1080/10420159908226199.

[14] D. Åberg, B. Sadigh, and P. Erhart, Physical Review B **85**, 125134 (2012), arXiv:arXiv:1201.3860v1.

[15] P. Dorenbos, E. van Loef, A. Vink, E. van der Kolk, C. van Eijk, K. Krämer, H. Güdel, W. Higgins, and K. Shah, Journal of Luminescence **117**, 147 (2006).

[16] S. Sato, Journal of the Physical Society of Japan **41**, 913 (1976), https://doi.org/10.1143/JPSJ.41.913.

[17] A. Canning and M. del Ben, Private communication.

[18] K. S. Song and R. T. Williams, *Self-Trapped Excitons*, Springer Series in Solid-State Sciences, Vol. 105 (Springer-Verlag, Berlin, Heidelberg, 1993).

[19] W. Drozdowski, P. Dorenbos, A. J. J. Bos, G. Bizarri, A. Owens, and F. G. A. Quarati, IEEE Transactions on Nuclear Science **55**, 1391 (2008).

[20] P. Dorenbos, Journal of Luminescence **136**, 122 (2013).

[21] P. Guss, M. E. Foster, B. M. Wong, F. Patrick Doty, K. Shah, M. R. Squillante, U. Shirwadkar, R. Hawrami, J. Tower, and D. Yuan, Journal of Applied Physics **115**, 034908 (2014), https://doi.org/10.1063/1.4861647.

[22] P. Dorenbos, Phys. Rev. B **85**, 165107 (2012).

[23] G. Bizarri and P. Dorenbos, Phys. Rev. B **75**, 184302 (2007).

[24] F. Quarati, P. Dorenbos, J. van der Biezen, A. Owens, M. Selle, L. Parthier, and P. Schotanus, Nuclear Instruments and Methods in Physics Research Section A: Accelerators, Spectrometers, Detectors and Associated Equipment **729**, 596 (2013).

[25] S. E. Derenzo, W.-S. Choong, and W. W. Moses, Physics in medicine and biology **59**, 32613286 (2014).

[26] S. Seifert, H. T. van Dam, and D. R. Schaart, Physics in medicine and biology **57**, 17971814 (2012).

[27] D. N. ter Weele, D. R. Schaart, and P. Dorenbos, IEEE Transactions on Nuclear Science **61**, 683 (2014).